

Crystallographic Studies on the Ribosome, a Large Macromolecular Assembly Exhibiting Severe Nonisomorphism, Extreme Beam Sensitivity and No Internal Symmetry

A. YONATH,^{a,b,*} J. HARMS,^{a,†} H. A. S. HANSEN,^a A. BASHAN,^b F. SCHLÜNZEN,^a I. LEVIN,^b I. KOELLN,^a A. TOCILI,^b I. AGMON,^b M. PERETZ,^b H. BARTELS,^a W. S. BENNETT,^a S. KRUMBHOLZ,^a D. JANELL,^a S. WEINSTEIN,^b T. AUERBACH,^b H. AVILA,^c M. PIOLLETTI,^c S. MORLANG^c AND F. FRANCESCHI^c

^aMax-Planck-Research Unit for Ribosomal Structure, Hamburg, Germany, ^bDepartment of Structural Biology, Weizmann Institute, Rehovot, Israel, and ^cMax-Planck-Institute for Molecular Genetics, Berlin, Germany.

E-mail: csyonath@weizmann.weizmann.ac.il

(Received 9 February 1998; accepted 23 July 1998)

Abstract

Crystals, diffracting best to around 3 Å, have been grown from intact large and small ribosomal subunits. The bright synchrotron radiation necessary for the collection of the higher-resolution X-ray diffraction data introduces significant decay even at cryo temperatures. Nevertheless, owing to the reasonable isomorphism of the recently improved crystals of the small ribosomal subunits, reliable phases have been extracted at medium resolution (5–6 Å) and an interpretable five-derivative MIR map has been constructed. For the crystals of the large subunits, however, the situation is more complicated because at higher resolution (2.7–7 Å) they suffer from substantial radiation sensitivity, a low level of isomorphism, instability of the longest unit-cell axis and nonisotropic mosaicity. The 8 Å MIR map, constructed to gain insight into this unusual system, may provide feasible reasoning for the odd combination of the properties of these crystals as well as hints for future improvement. Parallel efforts, in which electron-micro-

copy-reconstructed images are being exploited for molecular-replacement studies, are also discussed.

1. Introduction

The translation of the genetic code into polypeptide chains is a fundamental life process. In rapidly growing bacterial cells, the biosynthetic machinery constitutes about half of the dry weight of the cell and the biosynthetic process consumes up to 80% of the cell's energy. This intricate and essential process is performed by more than a hundred components, among which is the ribosome, the universal cellular organelle mediating the translation step of the biosynthetic process by catalyzing the sequential polymerization of amino acids according to the blueprint encoded in the mRNA. These giant nucleoprotein complexes (MW 2.3 MDa in prokaryotes and 4.5 MDa in mammals) are built of two independent subunits of unequal size, which associate on the initiation of protein biosynthesis. Each of the two ribosomal subunits carries different functional tasks and displays different structural properties. The large subunit catalyzes the formation of the peptide bond and provides the path along which the nascent protein progresses. The small subunit contains the site for the initiation of the translation step, facilitates the decoding of the genetic information and creates the features required for the *in vivo* selection mechanism. In prokaryotes, the molecular weights of the two ribosomal subunits are 1.45 and 0.85 MDa. About 1/3 of the mass of the prokaryotic ribosomes comprise 58–73 different proteins (21 in the small subunit and 37–52 in the large one, depending on its source). The other 2/3 are three chains of rRNA, of a total of about 4500 nucleotides (approximately 3000 and 1500 in the large and the small subunits, respectively).

Crystals have been grown from ribosomes, their complexes mimicking defined stages in protein biosynthesis, their natural, mutated, selectively depleted and chemically modified subunits (Berkovitch-Yellin *et al.*, 1992). Far beyond the initial expectations, two of

† The person who has made a significant contribution to these studies.

From its embryonic stages, ribosomal crystallography can be described as a series of barrier crossings, often associated with sharp turning points, requiring conceptual revisions and leading to unexpected developments. Nevertheless, Ada Yonath, together with her co-workers in Rehovot, Hamburg and Berlin, pioneered advanced procedures (e.g. cryo biocrystallography) and removed most of the obstacles. Consequently, electron-density maps at close to molecular resolution are currently emerging. Also, her starting model, proposed over a decade ago and creating serious doubts, as it contained internal features like tunnels and voids not detected previously, are now commonly accepted together with her interpretation. It is gratifying to see the increasing number of worldwide groups who are joining this area and willing to repeat her experiments.

these crystal forms, of the large subunit from *Haloarcula marismortui* (H50S) and of the small subunit from *Thermus thermophilus* (T30S), diffract currently to around 3 Å (Figs. 1 and 2, Table 1). Though this resolution range seems to be inferior to what is obtained from crystals of other large macromolecular complexes, for ribosomal crystals it should be considered rather

high in view of their enormous size, which does not contain any internal symmetry and the high level of their complexity.

It was found that the ribosomes are tough subjects for crystallographic analysis, primarily because they are composed of readily degradable RNA along with proteins which may be loosely held. Table 1 shows that, in contrast to the common observations, the high resolution obtained from the ribosomal crystals is not necessarily linked to diffraction of high quality. On the contrary, the crystal type diffracting to the highest resolution (H50S) yields the most problematic diffraction data. The efforts towards the elucidation of the structure of the ribosome and the problems (solved as well as unsolved) encountered over the years are the subjects of this article.

2. Radiation decay at cryo temperatures

The large unit-cell dimensions, the extremely weak diffraction power and the shape of the crystals (very thin plates or needles) dictate absolute dependence on synchrotron radiation. We pioneered crystallographic measurements at cryo temperatures because of the extreme radiation sensitivity of these crystals. Using moderate-intensity SR facilities, flash-frozen ribosomal crystals can be irradiated at 85–95 K with no observable damage for periods sufficient for the collection of an entire data set at 6–9 Å (in exceptional cases even at 5 Å) from individual crystals (Hope *et al.*, 1989). However, when evaluating these data it was observed

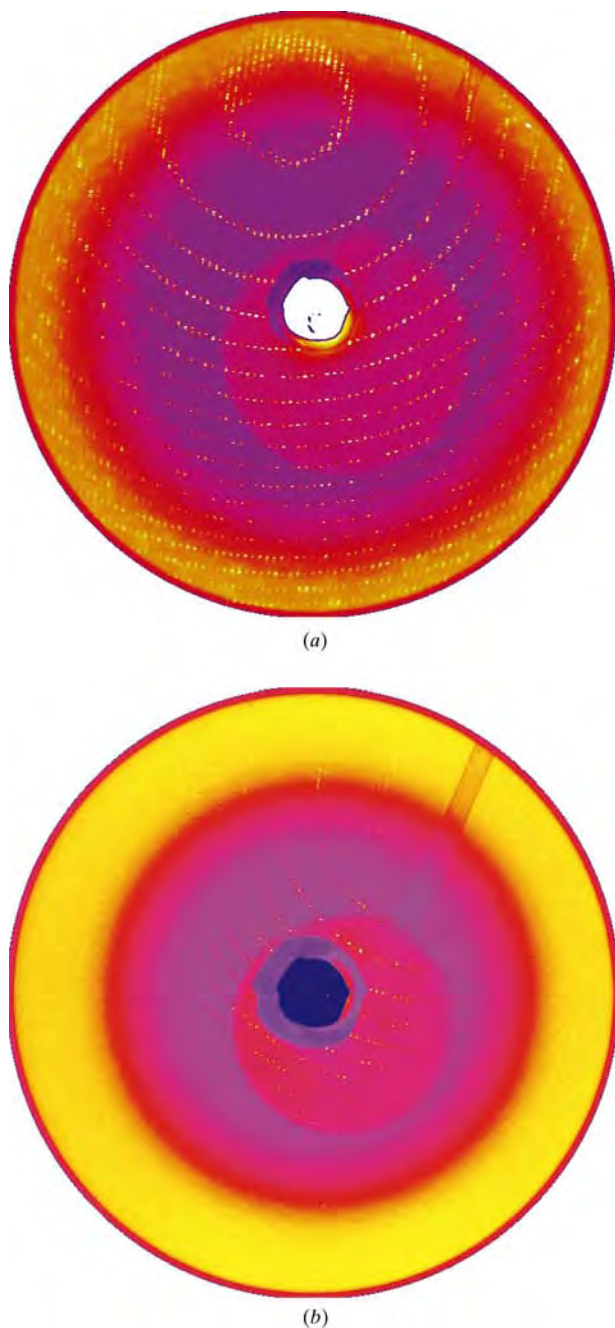


Fig. 1. Diffraction patterns (0.5° rotation) obtained within 20 s at the microfocus beamline (ID13) at ESRF from a crystal of H50S soaked in solution with 0.5 mM of W30. (a) The first pattern; (b) after 3.5° rotation.

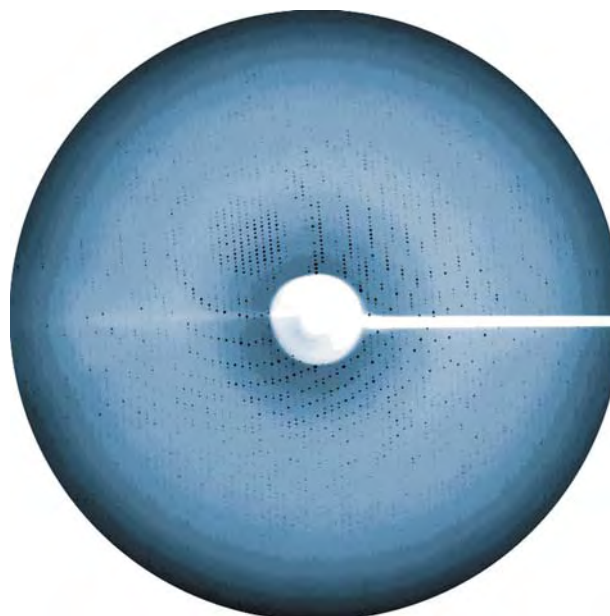


Fig. 2. A 1° rotation diffraction pattern obtained from a treated crystal of the small subunit from *Thermus thermophilus* (T30S) obtained at ID2/ESRF.

Table 1. *The quality of the ribosomal crystals*

T70S, T50S, T30S are the whole ribosome from *Thermus thermophilus* and its two subunits; H50S is the large subunit from *Haloarcula marismortui*

Source	Cell parameters (Å)	Resolution (Å)†	Isomorphism‡	Beam sensitivity§	Spot shape¶	Mosaicity††	Crystal shape and rigidity‡‡
T70S§§	524 × 524 × 306 <i>P</i> 4 ₁ 2 ₁ 2	12/15	OK	<i>U</i> ¶¶	OK	High	OK
T30S	407 × 407 × 170 <i>P</i> 4 ₁ 2 ₁ 2	3.5/3.9	OK	High	OK	Rather high	Thin, soft
T50S	495 × 495 × 196 <i>P</i> 4 ₁ 2 ₁ 2	8.7/9.5	OK	<i>U</i> ¶¶	OK	OK	OK
H50S	211 × 300 × 567 <i>C</i> 222 ₁	2.7/3.2	Hardly any	Very high	Deformed, elongated, nonuniform	Very high	Problematic

† The highest detectable/useful resolution. ‘Useful’ means 75% completeness (or higher) in the last shell. ‡ Isomorphism refers to native crystals grown from the same preparation. An OK indicates reasonable isomorphism for above 50% of the crystals. Very bad: less than 10% of the crystals are isomorphous (defined by cell dimensions and/or the distribution of the average $\Delta F/F$ values vs resolution). § Beam sensitivity at cryo temperature, using a bright synchrotron-radiation beam. ¶ An OK spot shape means that the reflections have a defined shape which corresponds to the shape of the crystals and to the cross section of the beam. Elongated and undefined shape indicates, in addition to these properties, a high chance for interpenetration. †† An OK corresponds to 0.2–0.5° mosaic spread. Very high may reach up to 3°. ‡‡ An OK means crystals of fairly isotropic dimensions which, when handled carefully, do not develop severe deformations. Problematic means extremely thin crystals, built from readily sliding layers, which, even upon extremely careful handling, may suffer from resolution loss and fragmentation. §§ A complex of T70S ribosomes, two phe-tRNA^{Phe} molecules and an oligomer of 35 uridines (as mRNA). The crystals of the pure T70S ribosome pack in the same crystal form but diffract only to 18/14 Å. ¶¶ Unknown or not well determined, since these crystals do not diffract to the resolution showing fast decay.

that, even in some cases for which the decay was not manifested in resolution loss, prominent damage was observed at the outer resolution shells. This ‘hidden’ decay is detectable in the data quality which becomes

poorer with the progression of the irradiation and is expressed in lower signal/noise ratios (*e.g.* from the original 9–10 to 2–3), higher R_{merge} values (*e.g.* from 0.06 to 0.17), fluctuations in the intraframe scaling factors

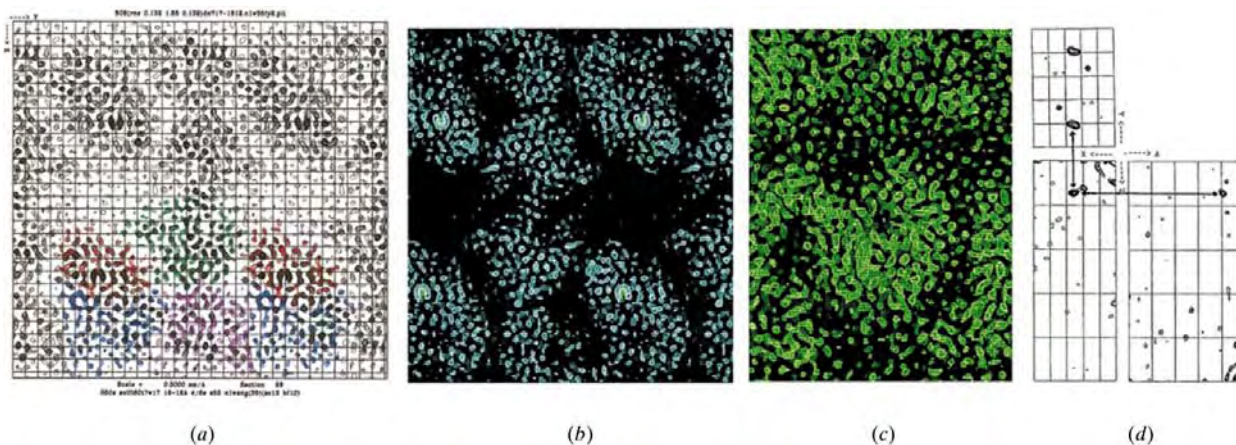


Fig. 3. (a) A stack of three sections, 3.3 Å apart, of the current 12 Å MIR map of H50S (211 × 300 × 567 Å, *C*222₁), showing the compact packing regions (around $z = 1/4$ and $3/4$) as well as the lonely contact area along the z axis [between the green particle and its symmetry-related (by twofold axis) noncolored one at $z = 1/2$, around the twofold axis]. For clarity, two unit cells are shown along the Y direction (horizontal) and the density assigned to the four asymmetric particles (+ two close neighbors) were painted red, blue, pink and green. The dense areas at the interface between the red and the blue particles represent the position of the most occupied heavy-atom sites. (b) The same map contoured at a higher level, in order to emphasize the solvent areas. (c) A part of the map oriented so that the entrance to the main ribosomal internal tunnel (Yonath *et al.*, 1987) is seen. (d) The $\text{Ta}_6\text{Br}_{14}$ difference-Patterson map of H50S, including the data of the 7.5–12.5 Å resolution shell. The corresponding Harker peaks are shown by arrows. Experimental details: over 11 000 reflections were measured, and a total of 15 heavy-atom sites of the three derivatives ($\text{Ta}_6\text{Br}_{14}$, W12 and W17; Table 2) were included. The positioning of the heavy-atom sites was performed by a combination of difference-Patterson and Fourier methods, based on the major position of $\text{Ta}_6\text{Br}_{14}$, found to be stable and consistent in all resolution ranges up to 6.5 Å (right). Each heavy-atom position was cross-verified and refined by *MLPHARE* with maximum likelihood. Since the contribution of the two W clusters was negligible beyond 10 Å, their scattering curve could be approximated by spherical averages of their corresponding radii (W18 = 10 Å and W12 = 8–9 Å). The $\text{Ta}_6\text{Br}_{14}$, however, was treated as in Knablein *et al.* (1997) owing to its potential for the higher-resolution shells. Mean FOM: 0.32 (0.57 for centric); R_{culis} : 0.76–0.97; phasing power: 0.98–1.15. The map was solvent flattened: one cycle, assuming 54% solvent.

between successive frames and frequent changes in the unit-cell dimensions.

It was firmly established that bright synchrotron radiation is essential for resolving the higher-resolution terms (above 6 Å). However, this high brightness (*e.g.* stations ID2 and ID13 at ESRF, ID19 at APS or F1 at CHESS) causes substantial radiation damage within a period sufficient for the collection of a few frames, hence dictating the construction of complete sets by merging data collected from several crystals. Coupled with the low level of isomorphism of the H50S crystals, this introduces extreme difficulties in the construction of complete data sets and in the interpretation of difference Patterson maps. Attempts at including the addition of various free-radical absorbers and/or at further cooling to He-stream temperatures (15–20 K) during data collection have so far made no significant improvement. Therefore, the crystals are irradiated part by part, using an X-ray beam of a cross section smaller than the crystal.

Experience showed that to obtain quality data from the higher-resolution shells extreme care in the pre-freezing treatment is required. In order to accommodate the delicate properties of the ribosomal crystals, namely the anisotropic morphology (at least one very thin edge), their notable softness and high bendability, procedures were developed for careful mounting of the crystals in a protective miniature double-layer thin glass spatula and for plunging the mounted spatula into liquid propane at its melting temperature (Hope *et al.*, 1989). The justification for using these rather complicated procedures was obtained five years later, when it was found that loop-mounted ribosomal crystals (Teng *et al.*, 1994) tend to float on the surface of the solvent bubble caught by the loop, bend around its concave shape and typically display lower resolution and a higher level of nonisomorphism.

3. Resolution versus diffraction quality

All crystals obtained so far from 70S ribosomes are characterized by their low resolution, 20–24 Å (Trakhanov *et al.*, 1987; Berkovitch-Yellin *et al.*, 1992), which probably stems from the inherent conformational heterogeneity of their preparations as they are extracted directly from cells during their growth phase. Based on this assumption, a complex mimicking a functional stage was designed and crystallized. Although this complex is rather unspecific [containing a short poly(U) chain and two charged tRNA^{phc} molecules], it led to a marked increase of the resolution, to 14–17 Å (Table 2 and Hansen *et al.*, 1990). Further improvement is expected from crystals of ribosomes programmed with mRNA chains of selected sequences, providing such complexes can remain stable throughout the crystallization period.

18 crystal forms have been grown from large ribosomal subunits, three of which were found to be suitable

for crystallographic analysis at various levels of detail. Among these, the crystals of the large ribosomal subunits from *Haloarcula marismortui* (H50S) have been the target of the most extensive crystallographic analysis, since they diffract to almost atomic resolution, 2.5–2.7 Å, and display reasonable mosaic spread (von Böhlen *et al.*, 1991). However, though data collected carefully at intermediate resolution led to MIR phasing (Fig. 3), it was found that the undesired properties of this crystal form (Table 1) become more problematic and less tolerable with the increase of resolution. For instance, at the higher-resolution ranges, the crystal decay is expressed not only by loss of resolution, which can be monitored visually, but also in an invisible, albeit substantial, growth of the longest unit-cell axis (Fig. 4). It is conceivable that each of the encountered problems could have been tolerated if they appeared in isolation. But the combination of severe nonisomorphism, high radiation sensitivity, nonstable cell constants, nonuniform mosaic spread, uneven reflection shape and high fragility, led in many cases to extreme difficulties even in the mere production of reliable data sets, let alone the construction and the interpretation of high-resolution difference Patterson maps.

It should be mentioned that in each preparation there are some crystals that lead to diffraction of reasonable mosaic spread (0.1–0.2°), nondeformed spot shape and no additional patterns (resulting from layer sliding). However, the level of isomorphism is very low even between these crystals and experience showed that the probability of detecting such crystals decreases with the increase of resolution (from 3–4% for those diffracting to 6–7 Å to 1–2% yielding high-quality diffraction to higher limits, 2.7–3.3 Å).

The 10–12 Å map presented in Fig. 3 and its extended 8 Å version, which shows a higher connectivity and can be partially interpreted (to be published), are based primarily on the contribution of a strong derivative, Ta₆Br₁₄. This derivative led to a well defined, and thus readily interpretable, difference Patterson map at 6.5 Å (Fig. 3) and consequently to the positioning of the sites of two other derivatives, W12 and W17 (Table 2). Noteworthy is the fact that the Ta₆Br₁₄-derivatized crystals diffract well to resolution much higher than the limits currently set by us, owing to the above described obstacles.

Interestingly, as expected, two prominent features of the large ribosomal subunit, the surface proteins L1 and L12, are poorly defined in the MIR map of H50S (Fig. 3). This is the consequence of an additional complication in studies of crystalline halophilic materials in ribosomes, for which the stabilization solution (3M KCl; von Böhlen *et al.*, 1991) is of electron density extremely close to that of 'average proteins', namely 0.38 electrons per Å³ [calculated from the values given by Anderson & Hovmöller (1998)]. Thus, at the medium-low resolution limits of current crystallographic studies, the limited

Table 2. *Metal clusters*

$R = \text{CH}_2\text{CH}_2\text{CONH}_2$; $R' = \text{CH}_2\text{CH}_2\text{CONHCH}_2\text{CH}_2\text{CONH}_2$;
 bu = butyl; ph = phenyl.

PIP = (diethylenamine)diododiplatinum(II)
 TAMM = tetrakis[(acetoxymercuro)methane]
 WAC = $\text{W}_3\text{O}_2 \cdot 3(\text{acetate}) \cdot 6\text{H}_2\text{O} \cdot \text{CFSO}_3$

$\text{Ta}_6\text{Cl}_{14}$
 $\text{Ta}_6\text{Br}_{14} \cdot 2\text{H}_2\text{O}$
 $\text{Nb}_6\text{Cl}_{14}$

$\text{Ir}_4(\text{CO})_8R'R''\dagger$
 $\text{C}_{22}\text{H}_{280}\text{N}_{24}\text{O}_{38}\text{P}_7\text{Au}_{11}\dagger$
 $\text{W}_{12}\text{Rh} = \text{CS}_5\text{H}_x\text{SiW}_{11}\text{O}_{39}\text{Rh}^{\text{III}}\text{CH}_3\text{COO}(\text{H})\dagger$

$\text{W}_{30} = \text{K}_{14}(\text{NaP}_5\text{W}_{30}\text{O}_{110}) \cdot 31\text{H}_2\text{O}$
 $\text{W}_{12} = \text{K}_5\text{H}(\text{PW}_{12}\text{O}_{40}) \cdot n\text{H}_2\text{O}$
 $\text{W}_{18} = (\text{NH}_4)_6(\text{P}_2\text{W}_{18}\text{O}_{62}) \cdot 14\text{H}_2\text{O}$
 $\text{W}_{17}\text{Co} = \text{CoWLi}_{17} = \text{Cs}_7[\text{P}_2\text{W}_{17}\text{O}_{61}\text{Co}(\text{NC}_5\text{H}_5)] \cdot n\text{H}_2\text{O}$
 $\text{BuSnW}_{17} = \text{K}_7[(\text{buSn})(\text{P}_2\text{W}_{17}\text{O}_{61})] \cdot n\text{H}_2\text{O}$
 $\text{PhSnW}_{15} = \text{K}_5\text{H}_4[(\text{phSn})_3(\text{P}_2\text{W}_{15}\text{O}_{59})] \cdot n\text{H}_2\text{O}$
 $\text{BuSnW}_{15} = \text{K}_5\text{H}_4[(\text{buSn})_3(\text{P}_2\text{W}_{15}\text{O}_{59})] \cdot n\text{H}_2\text{O}$
 $\text{Na}_{16}[(\text{O}_3\text{PCH}_2\text{PO}_3)_4\text{W}_{12}\text{O}_{36}] \cdot n\text{H}_2\text{O}$

† Can be used for covalent binding.

contrast of the ribosomal proteins causes their outline to merge with the solvent. The clarity at which the same features can be seen in the map phased by combined MR and SIRAS methods (Ban *et al.*, 1998) indicates the domination of phases, determined directly or according to the selectivity of molecular-replacement results obtained by using a model of artificially uniform density, although it is composed of over 66% RNA and only 34% proteins. Even at this resolution range, this MIR map may shed light on the odd combination of the properties of H50S. Thus, the potential high resolution obtained from the H50S crystals, 2.7 Å, may be accounted for by the extensive interparticle contacts which are concentrated in parts of the unit cell. At the same time, only one relatively small region, surrounded by a sizable volume of solvent with dimensions which may reach over 200 Å in their longest direction, is involved in contacts between the two halves of the unit cell along the very long *c*-axis (567 Å) direction. This rather unusual packing arrangement may be the reason for the low isomorphism of this crystal form, for the problematic morphology (plates reaching up to 0.5 × 0.5 mm with a typical thickness of a few micrometres in the direction of the *c* axis), for the layer structure of the crystals, for the high tendency of these layers to slide relative to each other (causing multilattice diffraction patterns), for the changes in the *c* axis which are introduced by irradiation (Fig. 4), and for the readiness of the penetration of very large clusters (*e.g.* W30, W18 *etc.*, see Table 2) into the crystals. Finally, although still uncertain, it seems that the lonely contact network is made by two symmetry-related particles *via* their 5S RNA regions (Levin *et al.*, 1998) and that a large part of the contacts can be interpreted as RNA chains

which form rather loose interparticle contacts, presumably mediated by the solvent. Hence, the influence of Mg and Cd ions on the rigidity of the crystals and their thickness may also be understood.

It should be mentioned that a similar packing arrangement was obtained independently by molecular replacement, exploiting the image reconstructed from T50S (Levin *et al.*, 1998). However, although this solution has reasonable scores (*i.e.* 93% correlation with *R* factor of 27% for the region > 60 Å and 48% correlation with *R* factor 42% for the region 30–90 Å), it is comparable to several other solutions. The use of the envelope of a ribosomal particle from one bacterium for determining the packing diagram of crystals grown from the same particle but from a different source is based on the assumption that at low resolution the gross structural features of prokaryotic ribosomes are rather similar. However, at higher resolution, the validity of such studies is questionable and the loss of scores with the advance of resolution may be accounted for by the difference between T50S and H50S (the latter contains 12–14 additional proteins), as well as the quality of the model.

Three packing arrangements have already been suggested for H50S crystals. The first was based on MIR and anomalous phase information, initially determined at 15 Å (Schlünzen *et al.*, 1995). The second (Roth *et al.*, 1996) and the third (Ban *et al.*, 1998), published during the reviewing stage of this manuscript, seem to be rather similar not only in their packing scheme but also in the way they were obtained. Thus, they originated from 30 Å non-MIR information, *i.e.* direct methods and molecular replacement, respectively, and so far could be validated only to low-resolution limits (*i.e.* 12–15 Å).

Apart from the general concern regarding the domination of the phases determined by molecular replacement or similar procedures, relying solely on phase

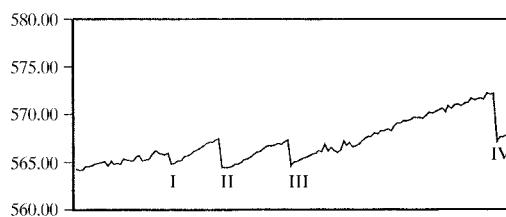


Fig. 4. The 'fluctuating' *c* axis. Data were collected sequentially from a crystal of the large ribosomal subunit (H50S) from *Haloarcula marismortui* (diffraction patterns shown in Fig. 1). The crystal size was 400 × 380 × 8 μm and the beam cross section 100 × 100 μm. The initial resolution was higher than 3.2 Å (at the edge of the MAR detector). The loss of resolution was monitored by eye inspection and when it reached 6–7 Å (points I, II, III) the crystal was translated to a new position (except for the position marked IV, at which the resolution limit was 9.5 Å). The region that was exposed last suffered from the decay of its neighbor even before it was exposed. As can be seen, the crystal decay was accompanied by an increase of the *c* axis, from 564 to 572 Å.

information originating from very low resolution information may be rather misleading. Thus, the use of procedures developed for systems possessing an extensive level of internal noncrystallographic symmetry and/or for the use of heavy-atom derivatives showing (potentially or in reality) phasing power extending near-molecular resolution (Jack *et al.*, 1975), is not always justified. This is so especially when the non-MIR information leads to the use of heavy-atom sites that were determined mainly by difference-Fourier methods and possess phasing power extending only to low resolution (*i.e.* 10–14 Å). Thus, at these resolution ranges the contribution to the structure factors of the noncrystalline material (the solvent) may reach the same order of magnitude as the contribution of the crystalline material. Therefore, using low-resolution phases for the location of heavy-atom sites by difference-Fourier methods might be strongly influenced by the solvent contribution, particularly in cases of heavy-atom clusters which possess phasing power extending only to low resolution. Consequently, the chances that the so determined heavy-atom sites may indeed represent changes in the solvent contribution are nonnegligible, even when they display acceptable phasing statistics (*e.g.* Schlünzen *et al.*, 1995).

This risk is especially high for the combination of ribosomal crystals with multi-tungsten clusters. In recent studies, it was found that significant amounts of W clusters, in quantities much higher than those directly incorporated in the phasing procedure (*i.e.* detected in difference-Patterson or Fourier maps), remain within the crystal environment even after applying an extensive washing procedure (12 times during 40–50 h). Thus, the amount of W atoms found in the washed crystals by inductively coupled plasma mass spectrometry as well as by atomic emission spectrometry is equivalent to 18–20 clusters of W₃₀ or to 25–27 clusters of W₁₈ per ribosomal particle. Such large amounts of 'floating' W clusters are sufficient to generate measurable anomalous signals by contributing to the structure factors, as well as to introduce subtle nonisomorphism, which may not be detected as such in routinely treated diffraction data. It therefore remains to be seen whether the bases for these three structures (Schlünzen *et al.*, 1995; Roth *et al.*, 1996; Ban *et al.*, 1998), *i.e.* the signals produced by these clusters at 12–15 Å were a consequence of real derivatization or of inherent or induced nonisomorphism or of the mere modification of the density of the crystal solvent.

In contrast to the marked tendency of large ribosomal subunits to crystallize, only one crystal form has been obtained so far from the small ribosomal subunit (Trakhanov *et al.*, 1987; Yonath *et al.*, 1988). For almost a decade, this crystal form (T30S) yielded satisfactory data only to 12–15 Å (Schlünzen *et al.*, 1995), although reflections were observed up to 7.3 Å. The low internal order of the crystals of the small ribosomal subunits was

correlated with their marked instability, which reaches a higher level than that observed for the large subunits. For example, by exposing 70S ribosomes to a potent proteolytic mixture, the 50S subunits remained intact, whereas the 30S subunits were completely digested. Similarly, large differences in the integrity of the two subunits were observed while attempting the crystallization of functionally active 70S ribosomes, constructed from purified subunits. Thus, the crystals obtained from these preparations were shown to consist only of 50S subunits (Berkovitch-Yellin *et al.*, 1992). This indicates that the self-affinity of the large subunits overcame their interactions with the small subunits to produce 70S particles not engaged in protein biosynthesis. Noteworthy is the fact that, at the end of this one week experiment, the supernatant of the crystallization drop did not contain intact small subunits but their proteins and their fragmented RNA chain. Thus, while the large subunits crystallized, the small ones deteriorated to their individual components.

Subtle modifications in the procedures of bacterial growth and crystal treatment led recently to useful diffraction to about 3.5 Å with reasonable, though far from perfect, isomorphism and reproducibility (Table 1). Large, medium-size and smaller metal compounds are being exploited for MIR and MAD phasing, leading typically to multisite binding which imposes extensive cross-verifications. This approach led to sufficient phasing power up to 6–6.3 Å resolution (limits currently dictated by the derivatized crystals) and allowed the construction of an interpretable electron-density map (to be published).

4. Facilitating specific derivatization

Single heavy-atom compounds yielded useful high-resolution phases for several large complexes. Among these are the viruses (*e.g.* Jack *et al.*, 1975, Rossmann, 1995), the 371K ATPase (Abrahams *et al.*, 1994) and the 250K tRNA^{Phe} synthetase and its complex with its cognate tRNA (Goldgur *et al.*, 1997). Compounds of three or four heavy atoms such as TAMM and PIP (Table 2) were the key for phasing the data of the 260K nucleosome-core particle (Luger *et al.*, 1997). Owing to the enormous size of the ribosome and the lack of internal symmetry, for generating accurately measured signals at low and medium resolution, advantage may be taken of compact and dense compounds containing several metals. In contrast to the availability of numerous single-atom agents, there are only a few stable water-soluble polymetallic compounds that may be suitable for derivatization. Examples are heteropolyanions or multicoordination compounds for soaking experiments and monofunctional reagents of dense metal clusters designed for covalent binding at specific sites [Thygesen *et al.* (1996) and Table 2].

With the increase of resolution of the ribosomal crystals, middle-size compounds were found useful.

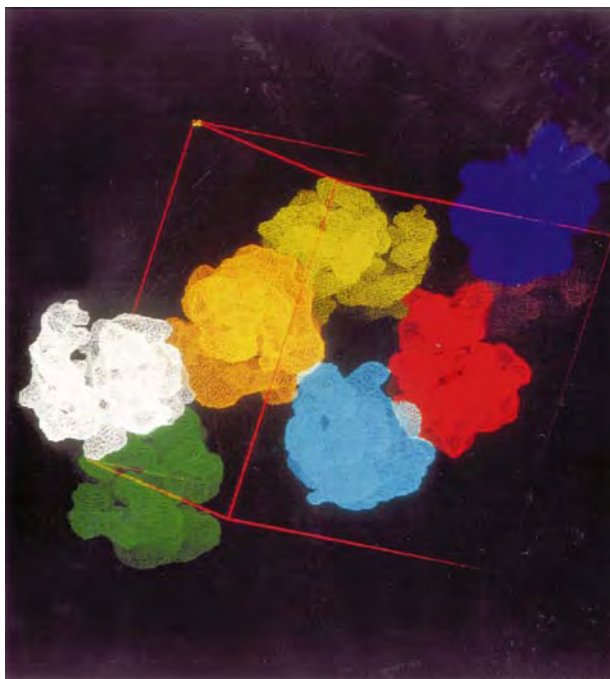


Fig. 5. The packing diagram of the whole ribosome (T70S), assembled by positioning the 23 Å electron-microscopical model in the crystallographic unit cell according to the most prominent result of the molecular-replacement search (crystallographic data were collected to 10 Å resolution).

Among these is $\text{Ta}_6\text{Cl}_{14}$, a compound that has recently become rather popular in macromolecular crystallography as it was shown to phase at different resolution ranges over a wide pH range (*e.g.* Schneider & Lindquist, 1994; Knablein *et al.*, 1997). In contrast, TAMM, which proved suitable for phasing data from crystals of rather large particles, such as the photosynthetic reaction center (Deisenhofer *et al.*, 1984), the nucleosome-core particle (Luger *et al.*, 1997), an iodotype-anti-iodotype complex (Bentley *et al.*, 1990) and glutathione transferase (Reinemer *et al.*, 1991), could not be exploited in ribosomal crystallography either because of low solubility (H50S) or because it introduces severe nonisomorphism (T30S and T50S). The situation with PIP, which was also used for phasing in some of the studies mentioned above (*e.g.* Luger *et al.*, 1997), is unclear. It obviously did not introduce substantial nonisomorphism, but at the same time its phasing power was found to be lower than that obtained from smaller compounds, showing presumably that it decomposes in an uncontrolled fashion during the course of the experiment.

In order to obtain a high occupancy of the heavy atoms, their quantitative attachment to predetermined sites prior to crystallization should be advantageous. The feasibility of phasing by specifically bound heavy atoms prior to the crystallization has been proven for the nucleosome-core particle at 2.8 Å (Luger *et al.*, 1997) and for B50S at low resolution (Bartels *et al.*, 1995). This approach requires complicated and time-consuming procedures but is bound to yield indis-

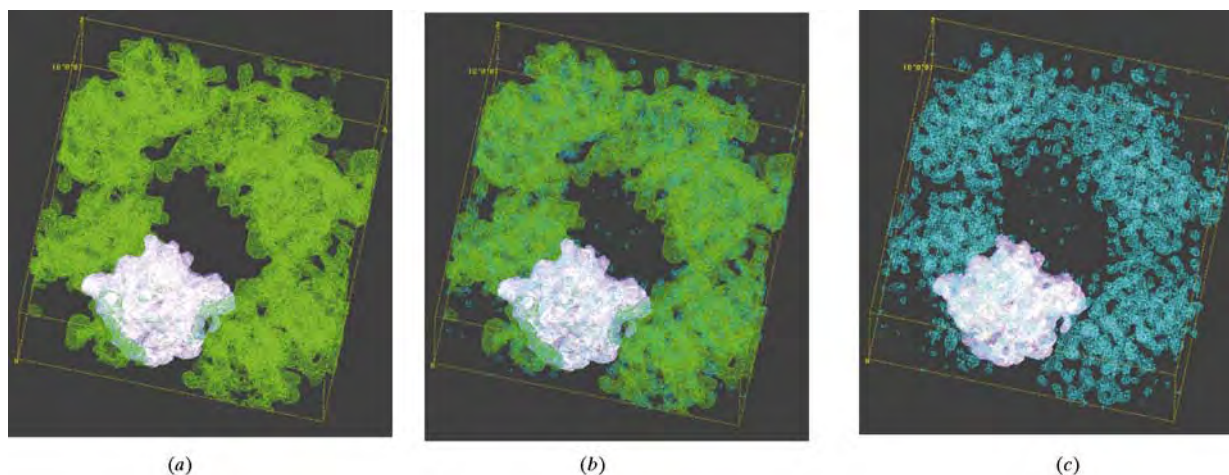


Fig. 6. The packing diagram of the large ribosomal subunit (T50S) assembled by positioning the 16 Å electron microscopical reconstructed image (Levin *et al.*, 1998) in the crystallographic unit cell according to the most prominent result of the molecular-replacement search. Structure-factor amplitudes and phases were calculated to 10 Å by back transformation. One asymmetric unit, which corresponds to one image, is marked in pink. (a) The map calculated from the amplitude and the phases of the model up to 10 Å resolution. The green patches on top of the model are parts of the neighboring particles. (b) The same map together with that constructed from the crystallographic amplitudes and the model phases (in cyan). The cyan patches that coincide with the green are of the neighboring particles. The 'only cyan' patches indicate differences in the structure between the observed and the calculated particles. (c) The 10 Å map constructed from F_{obs} and calculated (model) phases. [Up to 11 000 unique reflections (to 9 Å resolution) were collected from a native and $\text{Ta}_6\text{Br}_{14}$ derivatized crystals (measured at BW6/DESY at four wavelengths). Six heavy-atom sites were extracted from anomalous difference-Patterson maps (highest FOM = 0.7188, $R_{\text{cullis}} = 0.75$, phasing power = 1.56)].

pensable information not only for phasing but also at later stages of map interpretation. Examples of such materials are the clusters of undecatungsten (Wei *et al.*, 1998), undecagold and tetrairidium (Jahn, 1989*a,b*) (Table 2).

The studies on the structure of the nucleosome-core particle are illuminating. This particle consists of about 150 base pairs of DNA wrapped around an internal core composed of an octamer made of two copies of four histones. Since the fine characteristics of the structure of each individual nucleosome core is dictated by the sequence of the incorporated DNA (which varies as a function of its position on the genome), the crystals obtained from naturally occurring nucleosome-core particles exhibited structural variability and diffracted only to 7 Å (Richmond *et al.*, 1984). To introduce uniformity, a semiartificial nucleosome-core particle was designed, consisting of genetically produced histones together with a fragment of 146 base pairs, synthesized with a defined sequence. In addition to the provision of a homogenous population, the use of recombinant nucleosome cores facilitated the insertion of exposed cysteines at selected sites on the surface of the histone proteins.

This elegant and logical approach cannot be fully adopted for the derivatization of the ribosomes, since so far all the totally reconstructed ribosomal particles did not yield well diffracting crystals. This was rather unexpected since it is known that functionally active ribosomes can be reconstituted *in vitro* from isolated ribosomal components. It is conceivable that the *in vitro* assembly pathways lead to slight deviations from the natural conformation, sufficient to prohibit quality crystallization, because the conditions under which the reconstitution is performed *in vitro* are dramatically different from the physiological events (*e.g.* 1.5 h for *in vitro* reconstitution *versus* the *in vivo* 3 min). Therefore, binding heavy atoms to the ribosomes prior to their crystallization is limited either to available sites on the native particles or to the genetic creation of potential binding sites on selected ribosomal proteins that can be quantitatively and reversibly detached from the ribosome under mild conditions (Sagi *et al.*, 1995).

Phasing by MAD should eliminate the dependence on isomorphism, providing all the data can be collected from a single crystal. Owing to the severe radiation decay of the ribosomal crystals, this requirement cannot be fulfilled, but it is anticipated that even partial high-resolution phase information obtained from individual crystals should be more useful than that expected to be obtained from difference maps. The suitability of this method for ribosomal crystallography is currently being assessed and a word of caution is due, since the anticipated anomalous signals may be of the same order of magnitude as the changes in structure factors induced by the crystals' decay. MAD studies exploiting selenium gained recently a lot of popularity in protein crystal-

lography. For obtaining selenated halophilic ribosomal particles, a methionine-dependent strain was constructed (M. Mevarech, private communication). The 50S subunits of this strain yield crystals that may be of higher quality than those grown from the problematic H50S wild-type. The exact numbers of methionines in T30S and H50S are still to be determined, since only some of the sequences of the ribosomal proteins from these sources are known. Their estimated numbers (25 and 55, respectively) may not be sufficient to provide measurable signals, therefore efforts are being made to increase their amounts by genetic techniques (Franceschi *et al.*, 1993).

5. The interplay between microscopy and crystallography

In order to elucidate the packing arrangements of the ribosomal crystal forms that diffract to low resolution (T70S and T50S, see Table 1), molecular-replacement searches have been performed. Initially, the models reconstructed from electron micrographs of tilt series of negatively stained crystalline arrays (Yonath *et al.*, 1987; Arad *et al.*, 1987) were exploited. Recently, these studies were extended to higher resolution, benefiting from the impressive quantum jump in single-particle imaging by cryo electron microscopy (Stark *et al.*, 1995; Frank *et al.*, 1995), which yielded images resembling the common views observed by traditional electron microscopy and contain the features revealed in the lower-resolution reconstructed images from crystalline arrays.

Particles of the same preparations that yielded the best T50S and T70S crystals (Table 1) have been subjected to reconstruction at 16 and 23 Å resolution, respectively (Levin *et al.*, 1998). The molecular-replacement package *AMoRe* (Navaza, 1994) was chosen since it facilitates low-resolution work as it reads in models presented as density maps, a convenient feature when using electron-microscopy-reconstructed images. In both cases, a unique outstanding solution was obtained, showing no collisions or short contacts, with R_{merge} (I) of 41 and 45% and correlations of 75 and 72%, respectively (Figs. 5 and 6). An examination of the relations between the packing arrangement and the positions of the two most prominent Ta₆Br₁₄ sites determined by SIRAS from data collected at four wavelengths showed that one of them is located between two T50S particles and the second in a small nest within the T50S particle (Fig. 7). Parallel studies, exploiting a 24 Å reconstructed image of T30S (Levin *et al.*, 1998), led to a reasonable agreement with data collected from the 10 Å diffracting crystals (Levin *et al.*, 1998).

The anticipated (and encountered) immense difficulties in the determination of the structure of intact ribosomal particles led to parallel approaches, performed elsewhere, focusing on isolated ribosomal components. The substitution of the *E. coli* ribosome,

which used to be the favorable research object, by the more robust thermophilic particles, the employment of genetic techniques and the introduction of three-dimensional NMR spectroscopy, resulted in recent major progress in the determination of the molecular structures of isolated ribosomal proteins (for reviews, see Liljas & Al-Karadaghi, 1997; Hosaka *et al.*, 1997; Wimberly *et al.*, 1997) as well as RNA fragments (Betzler *et al.*, 1994; Puglisi *et al.*, 1997; Dallas & Moore, 1997; Correll *et al.*, 1997).

The relatively high level of detail of the reconstructed images tempted the fitting of ribosomal components of which the structures have been determined in isolation (*e.g.* Malhotra *et al.*, 1998) or those that can be approximated to known structures, such as double-stranded rRNA (Mueller & Brimacombe, 1997). An exercise to assess the feasibility of this approach, aiming at the fitting of the coordinates of a ribosomal protein TL1 (Nikonov *et al.*, 1996) into the electron-density map of large ribosomal subunits of the same organism (T50S) obtained by molecular replacement at 16 Å (Levin *et al.*, 1998), led to two alarming findings. The first is connected to the fact that a number of reasonable possibilities were obtained when the coordinates of the protein were manually placed in several orientations within the region assigned to be in the proximity of protein L1 by immuno electron microscopy. The second relates to a rather primitive molecular search, performed throughout the ribosomal particle, that revealed additional positions into which the same structure could be fitted equally well, indicating that currently unambiguous positioning of ribosomal components is still not possible. These studies also confirm the observation that protein L1 contains a popular RNA binding motif, detected in several ribosomal proteins (Nikonov *et al.*, 1996; Liljas & Al-Karadaghi, 1997). Additional uncertainties associated with such placements are due to the open questions concerning the validity of the conformations of ribosomal components determined in isolation to represent the *in situ* situation, since within the ribosome the individual components may be highly influenced by their proximity to other r-proteins or rRNA. An example is the isolated protein S15, which shows significant conformational variability between its structure in solution (determined by NMR) and in the crystal (Clemons *et al.*, 1998).

6. Some comparisons

A straightforward comparison between ribosomes and other macromolecular complexes of a size similar to (or larger than) that of the ribosome indicates that the size is a poor measure for the level of sophistication needed for structure determination. Indeed, the studies on viruses established that the readiness for structure determination is size independent and that significant structural irregularities can be overcome by focusing

only on the ordered part of the particle (*i.e.* neglecting the internal nucleic acids for the benefit of accurate determination of the structure of the coat proteins). In fact, the globular viruses, despite their enormous size, provide attractive crystallographic systems primarily because their surfaces are composed of readily packed proteins and because they possess extensive internal symmetry. Interestingly, the majority of the large macromolecular complexes so far subjected to structural analysis are composed mainly or solely of proteins (*e.g.* Deisenhofer *et al.*, 1984; Abrahams *et al.*, 1994; Knablein *et al.*, 1997; Xu *et al.*, 1997). Studies on the viruses and on the nucleosome (Luger *et al.*, 1997) show that a homogenous surface with defined and stable structural elements is the clue for efficient structure determination, no matter if this surface is composed on proteins or DNA. Combining these naive, albeit realistic, guidelines with the enormous size of the ribosomes and the extensive surface exposure of degradable RNA indicates that the ribosomes belong to a rather problematic group.

It is conceivable that the natural tendency of the ribosomes to deteriorate is one of the main sources for the severe complications in their structure determination. This is probably connected with the high content of surface RNA, prone to nucleolytic digestion. Intuitively, one may assume that the higher the extent of RNA fragmentation, the lower the quality of the resulting crystals. However, careful studies showed that although there may be an upper threshold for the number of breaks that can be tolerated by the crystallization process, as long as the crystallized particles are functionally active, a direct correlation between the quality of the crystals and the number of breaks in the rRNA could not be established.

7. Conclusions and prospectives

The increasing sophistication in instrumentation and in computational techniques and the implementation of powerful genetic techniques should provide the means to add the ribosomes to the list of complexes for which the structures have been solved. As shown, despite the long list of serious problems, the way to structure determination has been paved for the small subunit and is progressing for the large one. Thus, the quest for high-resolution structure under the conditions dictated by severe nonisomorphism, extreme radiation sensitivity and no internal symmetry may soon be reached.

8. Abbreviations

70S, 50S, 30S: the whole ribosome and its two subunits from prokaryotes. A letter as a prefix to the ribosomal particles or ribosomal proteins represents the bacterial source (*e.g.* E stands for *E. coli*; T for *Thermus thermophilus*; H for *Haloarcula marismortui*). tRNA, rRNA

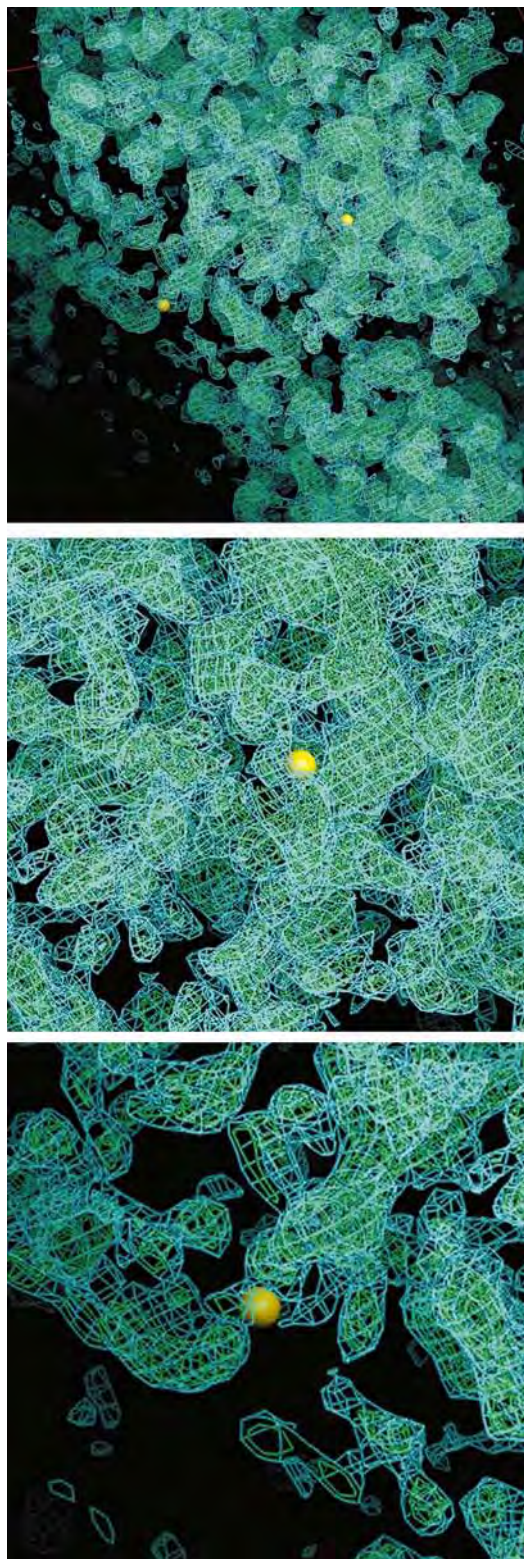


Fig. 7. A part of the map shown in Fig. 6, on which the positions of the most occupied Ta_6Br_{14} site are shown, represented as group scatterers with a diameter of about 6 Å (the golden balls) and two close-up views of these positions.

and mRNA stand for transfer, ribosomal and messenger RNA, respectively. r-proteins are ribosomal proteins, of which the names are composed of L or S (showing that this protein is of the large or small subunit) and a running number, according to the position of this protein on the two-dimensional gels. MIR: multiple isomorphous replacement. SIRAS: single isomorphous replacement with anomalous scattering. MAD: multiple anomalous dispersion. SR: synchrotron radiation. MR: molecular replacement.

Exceptional gratitude is due to the late Professor H. G. Wittmann with whom these studies were initiated. We thank Dr M. Safro for active participation in the phasing attempts, Drs M. Pope, W. Preetz and W. Jahn who gave us generous gifts of heavy-atom clusters, Drs M. van Heel and H. Stark for the reconstructions of the thermophilic ribosomal particles and Dr M. Mevarech for the methionine-dependent strain. The studies presented here were performed at the Weizmann Institute, Rehovot, the Max-Planck Research Unit in Hamburg and the Max-Planck Institute for Molecular Genetics in Berlin. We thank C. Radzwill, R. Albrecht, C. Glotz, Y. Halfon, K. Knaack, M. Laschever, S. Meier, J. Muessig, C. Paulke, U. Solomon and G. Arad for their assistance. Data were collected at the EMBL and MPG beam lines at DESY, Hamburg, F1/CHESS, Cornell University, ID2, ID13, D2AM/ESRF, Grenoble, BL26/PF/KEK, Japan, and ID19/APS. Support was provided by the Max-Planck Society, the US National Institute of Health (NIH GM 34360), the German Ministry for Science and Technology (BMBF 05-641EA) and the Kimmelman Center for Macromolecular Assembly at the Weizmann Institute. AY holds the Martin S. Kimmel Professorial Chair.

References

- Abrahams, J. P., Leslie, A. G. W., Lutter, R. & Walker J. E. (1994). *Nature (London)*, **370**, 621–628.
- Anderson, K. M. & Hovmöller, S. (1998). *Z. Kristallogr.* **213**, 369–373.
- Arad, T., Piefke, J., Weinstein, S., Gewitz, H. S., Yonath, A. & Wittmann, H. G. (1987). *Biochimie*, **69**, 1001–1006.
- Ban, N., Freeborn, B., Nissen, P., Penczek, P., Graussucci, R. A., Sweet, R., Frank, F., Moore P. & Steitz, T. (1998). *Cell*, **93**, 1105–1115.
- Bartels, H., Bennett, W. S., Hansen, H. A. S., Eisenstein, M., Weinstein, S., Muessig, J., Volkmann, N., Schlünzen, F., Agmon, I., Franceschi, F. & Yonath, A. (1995). *J. Pept. Sci.* **37**, 411–419.
- Bentley, G. A., Boulot, G., Riottot, M. M. & Poljak, R. J. (1990). *Nature (London)*, **348**, 254–257.
- Berkovitch-Yellin, Z., Bennett, W. S. & Yonath, A. (1992). *Crit. Rev. Biochem. Mol. Biol.* **27**, 403–446.
- Betz, C., Lorenz, S., Fürste, J. P., Bald, R., Zhang, M., Schneider, T. R., Wilson, K. S. & Erdmann, V. A. (1994). *FEBS Lett.* **351**, 159–164.

- Böhlen, K. von, Makowski, I., Hansen, H. A. S., Bartels, H., Berkovitch-Yellin, Z., Zaytzev-Bashan, A., Meyer, S., Paulke, C., Franceschi, F. & Yonath, A. (1991). *J. Mol. Biol.* **222**, 11–15.
- Clemons, W. M., Davies, C., White, S. & Ramakrishnan, V. (1998). *Structure*, **6**, 429–438.
- Correll, C. C., Freeborn, B., Moore, P. B. & Steitz, T. A. (1997). *Cell*, **91**, 705–712.
- Dallas, A. & Moore, P. B. (1997). *Structure*, **5**, 1639–1653.
- Deisenhofer, J., Epp, O., Miki, K., Huber, R. & Michel, H. (1984). *J. Mol. Biol.* **180**, 385–398.
- Franceschi, F., Weinstein, S., Evers, U., Arndt, E., Jahn, J., Hansen, H. A. S., von Böhlen, K., Berkovitch-Yellin, Z., Eisenstein, M., Agmon, I., Thygesen, J., Volkmann, N., Bartels, H., Schlünzen, F., Bashan, A., Sharon, R., Levin, I., Dribin, A., Sagi, I., Choli-Papadopoulou, T., Tsiboly, P., Kryger, G., Bennett, W. S. & Yonath, A. (1993). *The Translational Apparatus*, edited by K. Nierhaus, pp. 397–410. New York: Plenum Press.
- Frank, F., Zhu, J., Penczek, P., Li, Y., Srivastava, S., Verschoor, A., Radamacher, M., Grassucci, R., Lata, A. K. & Agrawal, R. K. (1995). *Nature (London)*, **376**, 441–444.
- Goldgur, Y., Mosyak, L., Reshetnikova, L., Ankilova, V., Lavrik, O., Khodyreva, S. & Safro, M. (1997). *Structure*, **5**, 59–69.
- Hansen, H. A. S., Volkmann, N., Piefke, J., Glotz, C., Weinstein, S., Makowski, I., Meyer, S., Wittmann, H. G. & Yonath, A. (1990). *Biochem. Biophys. Acta*, **1050**, 1–5.
- Hope, H., Frolow, F., von Böhlen, K., Makowski, I., Kratky, C., Halfon Y., Danz, H., Webster, P., Bartels, K., Wittmann, H. G. & Yonath, A. (1989). *Acta Cryst.* **B45**, 190–198.
- Hosaka, H., Nakagawa, A., Tanaka, I., Harada, N., Sano, K., Kimura, M., Yao, M. & Wakatsuki, S. (1997). *Structure*, **5**, 1199–1208.
- Jack, A., Harrison, S. C. & Crowthers, R. A. (1975). *J. Mol. Biol.* **97**, 163–172.
- Jahn, W. (1989a). *Z. Naturforsch. Teil B*, **44**, 79–82.
- Jahn, W. (1989b). *Z. Naturforsch. Teil B*, **44**, 1313–1322.
- Knablein, J., Neufelnd, T., Schneider, F., Bergner, A., Masserschmidt, A., Löwe, J., Steipe, B. & Huber, R. (1997). *J. Mol. Biol.* **270**, 1–7.
- Levin, I., Tocilj, A., Agmon, I., Koelln, I., Stark, H., Cuff, M., Van Heel, M., Schlünzen, F., Bashan, A., Franceschi, F. & Yonath, A. (1998). Submitted.
- Liljas, A. & Al-Karadaghi, S. (1997). *Nature Struct. Biol.* **4**, 767–771.
- Luger, K., Maeder, A. W., Richmond R. K., Segent, D. F. & Richmond, T. J. (1997). *Nature (London)*, **389**, 251–260.
- Malhotra, A., Penczek, P., Agrawal, R. K., Gabashvili, I. S., Grassucci, R. A., Junemann, R., Burkhardt, N., Nierhaus, K. H. & Frank, J. (1998). *J. Mol. Biol.* In the press.
- Mueller, F. & Brimacombe, R. (1997). *J. Mol. Biol.* **271**, 524–544.
- Navaza J. (1994). *Acta Cryst.* **A50**, 157–163.
- Nikonov, S., Nevskaya, N., Eliseukina, I., Fomenkova, N., Nikulin, A., Ossina, N., Garber, M., Jonsson, B.-H., Briand, C., Al-Kadaghi, S., Svensson, A., Aevvarsson, A. & Liljas, A. (1996). *EMBO J.* **15**, 1350–1359.
- Puglisi, E. V., Green, R., Noller, H. F. & Puglisi, J. D. (1997). *Nature Struct. Biol.* **4**, 761–772.
- Reinemer, P., Dirr, H. W., Ladenstein, R., Schaeffer, J., Gally, O. & Huber, R. (1991). *EMBO J.* **10**, 1997–2005.
- Richmond, T. J., Finch, J. T., Ruston, B., Rhodes, D. & Klug, A. (1984). *Nature (London)*, **311**, 532–537.
- Rossmann, M. G. (1995). *Curr. Opin. Struct. Biol.* **5**, 650–655.
- Roth, M., Pebay-Peyroula, E., Bashan, A., Berkovitch-Yellin, Z., Agmon, I., Franceschi, F., Lewit-Bentley, A. & Yonath, A. (1996). *Biological Structure and Dynamics*, edited by R. H. Sarma & M. H. Sarma. Proceedings of the 9th Conversation, pp. 15–24. New York: Adenine Press.
- Sagi, I., Weinrich, V., Levin, I., Glotz, C., Laschever, M., Melamud, M., Franceschi, F., Weinstein, S. & Yonath, A. (1995). *Biophys. J.* **55**, 31–41.
- Schlünzen, F., Hansen, H. A. S., Thygesen, J., Bennett, W. S., Volkmann, N., Levin, I., Harms, J., Bartels, H., Bashan, A., Berkovitch-Yellin, Z., Sagi, I., Franceschi, F., Krumbholz, S., Geva, M., Weinstein, S., Agmon, I., Bøddeker, N., Morlang, S., Sharon, R., Dribin, A., Peretz, M., Weinrich, V. & Yonath, A. (1995). *J. Biochem. Cell Biol.* **73**, 739–749.
- Schneider, G. & Lindquist, Y. (1994). *Acta Cryst.* **D50**, 186–191.
- Stark, H., Mueller, F., Orlova, E. V., Schatz, M., Dube, P., Erdemir, T., Zenin, F., Brimacombe, R. & Van Heel, M. (1995). *Structure*, **3**, 815–821.
- Teng, T. Y., Schildkamp, W., Dolmer, P. & Moffat, K. (1994). *J. Appl. Cryst.* **27**, 133–137.
- Thygesen, J., Weinstein, S., Franceschi, F. & Yonath, A. (1996). *Structure*, **4**, 513–518.
- Trakhanov, S. D., Yusupove, M. M., Agalarov, S. C., Garber, M. B., Ryazantsev, S. N., Tichenko, S. V. & Shirokov, V. A. (1987). *FEBS Lett.* **220**, 319–322.
- Wei, X., Dickman, M. H. & Pope M. T. (1998). *J. Am. Chem. Soc.* In the press.
- Wimberly, T. W., White, S. W. & Ramakrishnan, V. (1997). *Structure*, **5**, 1187–1198.
- Xu, Z., Horwich, A. L. & Sigler, P. B. (1997). *Nature (London)*, **388**, 741–750.
- Yonath, A., Glotz, C., Gewitz, H. S., Bartels, K., von Böhlen, K., Makowski, I. & Wittmann, H. G. (1988). *J. Mol. Biol.* **203**, 831–833.
- Yonath, A., Leonard, K. R. & Wittmann, H. G. (1987). *Science*, **236**, 813–817.